



HAL
open science

Mapping inversion domain boundaries along single GaN wires with Bragg coherent X-ray imaging

L. Ni, Stéphane Labat, Steven Leake, Maxime Dupraz, Jérôme Carnis, Thomas W Cornelius, Guillaume Beutier, Marc Verdier, Vincent Favre-Nicolin, Tobias Schüllli, et al.

► To cite this version:

L. Ni, Stéphane Labat, Steven Leake, Maxime Dupraz, Jérôme Carnis, et al.. Mapping inversion domain boundaries along single GaN wires with Bragg coherent X-ray imaging. *ACS Nano*, 2020, 14 (8), pp.10305-10312. 10.1021/acsnano.0c03775 . hal-02916267

HAL Id: hal-02916267

<https://hal.science/hal-02916267>

Submitted on 22 Nov 2021

HAL is a multi-disciplinary open access archive for the deposit and dissemination of scientific research documents, whether they are published or not. The documents may come from teaching and research institutions in France or abroad, or from public or private research centers.

L'archive ouverte pluridisciplinaire **HAL**, est destinée au dépôt et à la diffusion de documents scientifiques de niveau recherche, publiés ou non, émanant des établissements d'enseignement et de recherche français ou étrangers, des laboratoires publics ou privés.

Mapping Inversion Domain Boundaries in Single GaN Wires

L. Ni,^{1,2} S. Labat,³ S. J. Leake,² M. Dupraz,^{1,2} J. Carnis,⁴ T. W. Cornelius,³ G. Beutier,^{5,6} M. Verdier,^{5,6} T. U. Schüllli,² O. Thomas,³ J. Eymery,¹ and M.-I. Richard¹

¹Univ. Grenoble Alpes, CEA Grenoble, IRIG, MEM, NRS, 17 rue des Martyrs 38000 Grenoble, France

²ESRF - The European Synchrotron, 71 Avenue des Martyrs, Grenoble 38000, France

³Aix Marseille Université, CNRS, Université de Toulon, IM2NP UMR 7334, 13397 Marseille, France

⁴Deutsches Elektronen-Synchrotron (DESY), D-22607 Hamburg, Germany

⁵Univ. Grenoble Alpes, SIMAP, F-38000 Grenoble, France

⁶CNRS, SIMAP, F-38000 Grenoble, France

(Dated: 15 January 2020)

Gallium nitride (GaN) is of technological importance for a wide variety of optoelectronic applications. Defects in GaN, like inversion domain boundaries (IDBs), significantly affect the electrical and optical properties of the material. We report, here, on the structural configurations of planar inversion domain boundaries inside n-doped GaN wires measured by Bragg coherent x-ray diffraction imaging. Different complex domain configurations are revealed along the wires with a 6-nm in-plane spatial resolution. We demonstrate that the IDBs change their direction of propagation along the wires, promoting Ga-terminated domains and stabilising into $\{1-100\}$ or m -planes. The atomic phase shift between the Ga- and N- terminated domains has been extracted using phase retrieval algorithms, revealing a slight evolution (~ 1 pm) of the out-of-plane displacement between inversion domains along the wire. This work provides an accurate inner view of planar defects inside small crystals.

Group-III nitrides play an important role as electronic and optoelectronic materials. Their wide bandgaps enable applications in blue-UV light emitting diodes, lasers and power devices or for photocatalysis.^{1,2} Among all the group-III nitride materials, GaN has a particular importance owing to its outstanding luminescence efficiency even with a high density of extended defects.³ Due to the lack of suitable substrate with a similar lattice parameter, GaN typically exhibits a high defect density when grown epitaxially. Of many possible defects, inversion domain boundaries (IDBs), across which cation and anion positions are interchanged, can be used to manipulate device performance associated with properties such as spontaneous polarization and Hall mobility.⁴ The increasing demand to reduce the dimensions of electronic devices makes GaN wires more interesting. The small contact area between wire and substrate allows wires to relax easily and fewer dislocations will be introduced.⁵ The wire morphology also improves the performance of flexible LEDs because of their mechanical flexibility⁶ and wave guiding properties.⁷ Characterisation of GaN wires in three-dimensions (3D) and at nanometer resolution are crucial to gain an understanding of the structure and the growth mechanisms of the wires and their inner defects. Defects in GaN wires are a key issue. Their study may give new insight into the optoelectronic properties of nitride semiconductors. Instead of traditional techniques, such as transmission electron microscopy (TEM) and scanning electron microscopy (SEM), Bragg coherent x-ray diffraction imaging (BCDI) was chosen in this work, for this technique can image defects, displacement and strain fields without destroying the sample or modifying it during the image acquisition process.⁸⁻¹¹

In this letter, we report Bragg coherent diffraction imaging of IDBs in GaN wires grown on sapphire. BCDI was used to investigate the arrangement of the IDBs inside the GaN wires and the displacement field generated by these defects

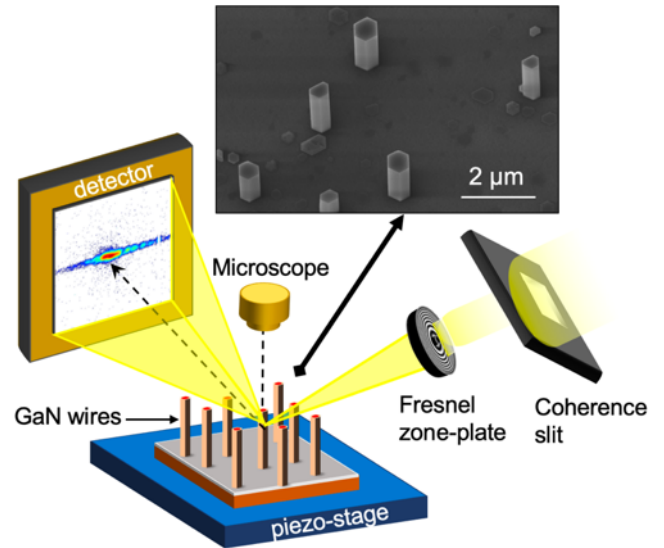


FIG. 1. Schematic overview of the experimental setup. The x-ray beam is focused using a Fresnel zone-plate. A microscope is positioned above the sample. The inset displays a scanning electron microscope (SEM) image of the GaN wires.

as a function of growth axis. Our results provides clues of the evolution and propagation of IDBs along the wire.

The samples consist of self-catalysed GaN wires grown on c -plane sapphire substrates by metal organic vapor phase epitaxy (MOVPE) (see Ref.⁹ for more information). Adjusting the growth conditions for BCDI studies allow to achieve a low density ($\sim 10^6 \text{ cm}^{-2}$) of wires with a length ranging from 3 to 5 μm and an average diameter of 600 nm, as illustrated by the scanning electron microscope (SEM) image of Fig. 1. The wires have their c -axis parallel or antiparallel to the growth

axis and lateral $\{1\bar{1}00\}m$ -plane facets. This work focuses on several different GaN wires (three in total), noted *A*, *B* and *C* hereafter. The silane concentration has been varied during the growth of wires *B* and *C*. This was not the case for wire *A*, for which a constant silane concentration was used during growth. BCDI was performed using a nano-focused x-ray beam at beamline ID01 of the European Synchrotron Facility (ESRF) in Grenoble (France) (see more details in Ref.⁹). BCDI was used to investigate the arrangement of the IDBs inside the GaN wires and the displacement field generated by these defects. The experimental setup is shown in Fig. 1.

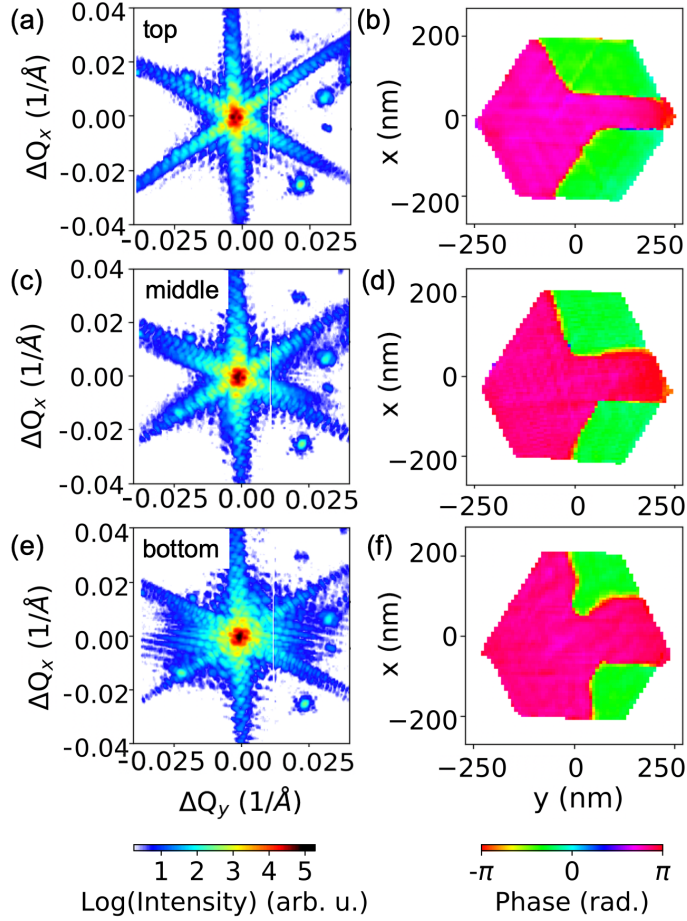


FIG. 2. Coherent x-ray diffraction measurements of the 004 GaN Bragg peak (left) and their associated real space reconstruction of the phase (right) at the top (a-b), center (c-d) and bottom (e-f) of wire *A*, respectively

Three-dimensional diffraction patterns were collected at three different z -positions (z being along the wire axis) along the different wires and at the 004 GaN Bragg reflection, while illuminating a portion (~ 400 nm thick corresponding to the vertical beam size (FWHM)) of the wire. To measure the full 3D diffraction patterns, the wires were rotated by 1.28° in steps of 0.005° . The distance between adjacent diffraction patterns are $1.5 \mu\text{m}$ for wire *A* and $1 \mu\text{m}$ for wires *B* and *C*. In all 3D diffraction patterns, the measured intensity is concentrated in an (h, k) -plane perpendicular to the l -axis. As

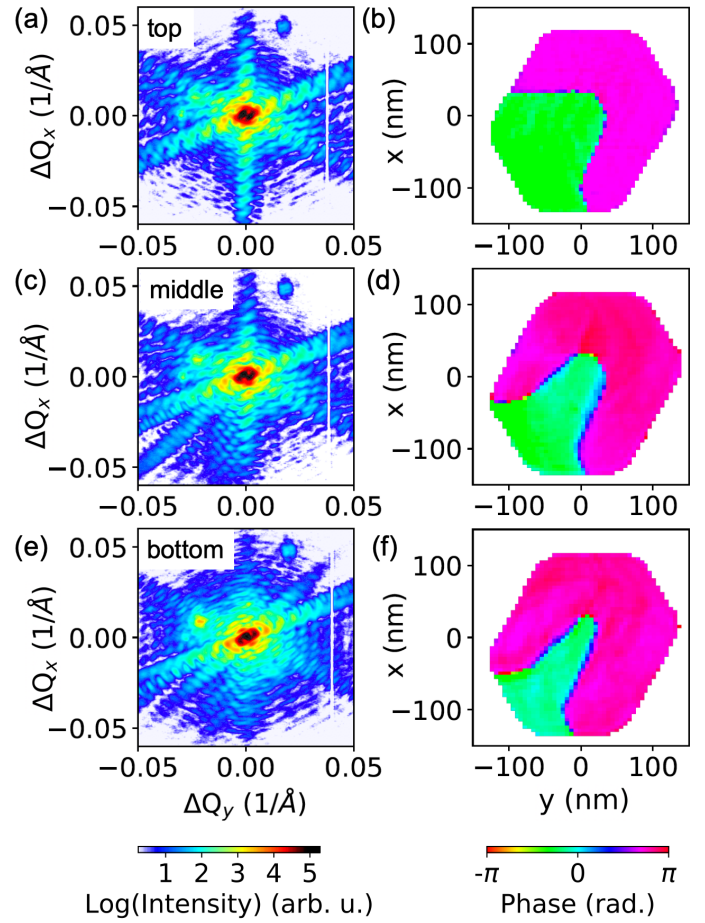


FIG. 3. Coherent x-ray diffraction measurements of the 004 GaN Bragg peak (left) and their associated real space reconstruction of the phase (right) at the top (a-b), center (c-d) and bottom (e-f) of wire *B* respectively.

reported in Ref.⁹, the 2D cross-section of the measured portion of the wire is supposed to be constant along the wires axis. 2D intensity maps are thus extracted from the 3D data sets to reconstruct a 2D image of the sample (see Figs. 2, 3 and 4 - right side (b, d and f)). The images correspond to the projection of the measured 3D portion along the c -axis of the wire onto 2D.

Figures 2, 3 and 4 (a, c and e) display coherent x-ray diffraction measurements as a function of the in-plane coordinates of the scattering vector \vec{Q} (Q_x and Q_y) at z -positions along the wires. Interestingly, the measurements (*i.e.* the diffraction patterns) are different from one wire to another. But they show some similarities, like six streaks demonstrating the hexagonal shape of the wires. The diffraction patterns along each wire (*i.e.*, at different z -positions) are also different, showing that their structure evolves along the wire for all of them. The diffraction patterns are more complex at the bottom of the wires, as expected, due to the dislocation network at the interface between the GaN wire and the substrate. Each diffraction pattern was used independently to reconstruct the inner structure of the wires using phase retrieval algorithms.

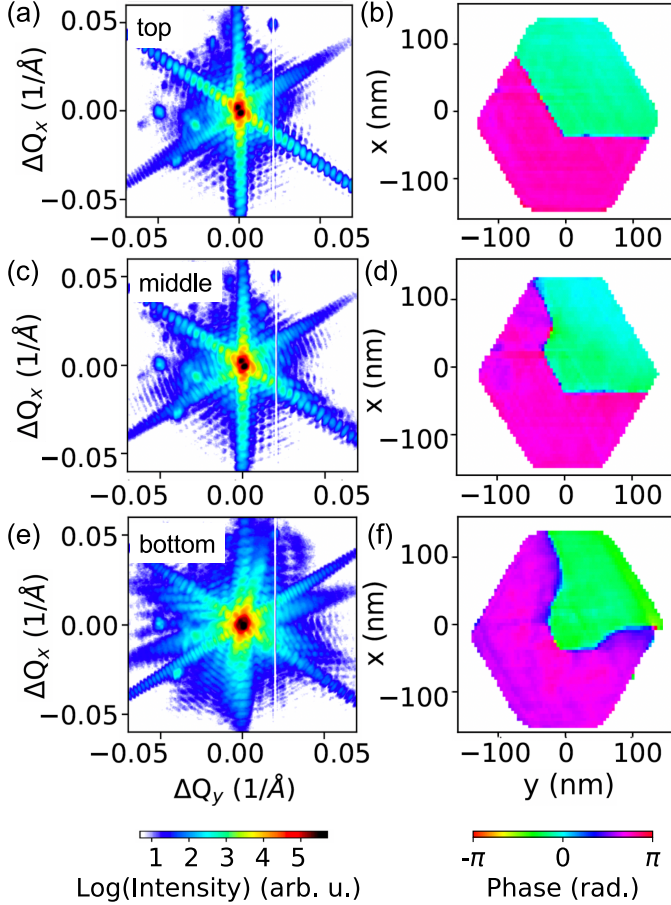


FIG. 4. Coherent x-ray diffraction measurements of the **004** GaN Bragg peak (left) and their associated real space reconstruction of the phase (right) at the top (a-b), center (c-d) and bottom (e-f) of wire *C* respectively.

Phase retrieval was carried out on the diffraction data using PyNX package,¹² imposing at each iteration that the calculated Fourier intensity of the guessed object, $\tilde{\Omega}(\vec{r})$, agrees with the measured data, I^{meas} . Signal from other wires observed in the measured data are masked. Gaps between the detector chips were masked: first set to zero and then set free during the phase retrieval procedure. Starting with random objects, 1200 iterations of Relaxed Averaged Alternating Reflections (RAAR¹³) and 300 iterations of Error-Reduction (ER^{14,15}) algorithms were applied with shrink-wrap¹⁶ algorithm (every 20 iterations) in each phasing process. After repeating several times, a support was drawn from the best reconstructed object. With this support as a starting support, it converges faster to the expected real-space object. Afterwards, the support was fixed, and it converges fairly well with 600 iterations of Hybrid Input Output (HIO¹⁷), RAAR and 300 iterations of ER. Although the support is fixed, the starting phase before each phasing process is totally random. Therefore, the generated phases are slightly different with each other. This is inevitable on account of noise caused by the detector. To select good results, the Poisson Log-Likelihood (LLK)¹⁸ is used

as a parameter, which indicates the quality of phasing. LLK is defined as:

$$LLK = -\frac{1}{N} \sum_i \log \left[\frac{(I_i^{calc})^{I_i^{meas}}}{I_i^{meas}!} e^{-I_i^{calc}} \right], \quad (1)$$

where N is the total number of pixels in the diffracted data, I_i^{meas} and I_i^{calc} denote the measured and calculated intensity at pixel i . LLK reflects the similarity of calculated and observed intensities. Reconstructed objects with lower LLKs have more homogeneous phases and sharper boundaries between the inversion domains. The true object $\tilde{\Omega}(\vec{r})$ as well as its twin-image $\tilde{\Omega}^*(-\vec{r})$, also called enantiomorph, are parts of the reconstructed solutions, since they have the same intensity in reciprocal space and since the shape of the reconstructed object is centrosymmetric. However, recognition of the twin-image is crucial to obtain the correct phase shift between the inversion domains, as the phase of the twin-object is opposite to the correct phase. As demonstrated by Labat *et al.*,⁹ they can be distinguished by considering the effect of the optical path length on the phase distribution. Considering that photons will travel different distances d inside the wire with respect to its geometry, the phase of the beam is shifted negatively by $-\frac{2\pi}{\lambda} \delta d$ (in our case, the maximum shift induced by the optical path is -0.2 rad.),¹⁹ where δ describes the dispersive part of the complex refractive index n of the material: $n = 1 - \delta + i\beta$. Longer optical path length results in a lower phase. Perpendicularly to the beam direction, a negative curvature of the phase is expected in the middle of the wire. This signature allows to select the correct solutions and discard the twin-image variants.

Figures 2, 3 and 4 (b, d and f) display the best reconstructed images of the wires at different z -positions. Two domains of different constant phase values (colored in pink and green) are observed. The domains are reconstructed with a pixel size of 6 (x -direction) \times 8.5 (y -direction) nm^2 for wire *A*, a pixel size of 4.9 (x -direction) \times 5.6 (y -direction) nm^2 for wire *B* and a pixel size of 5.1 (x -direction) \times 4.2 (y -direction) nm^2 for wire *B*. They correspond to domains of different polarities, either Ga (+ c) or N ($-c$) terminated domains, separated by inversion domain boundaries as reported in Ref.⁹

Figure 5(a) displays the raw and corrected values of the phase distribution along the y -axis of the reconstructed top cross-section of wire *B* (see Fig. 3(b)). To get a correct phase-shift from the retrieved phases, phase impacted by the optical path is corrected and the phase-ramp is removed. Removal of the phase-ramp is achieved by performing linear-regression on the two domains one by one and by calculating the weighted mean slope. Histograms of the raw and corrected phase distributions are displayed in Fig. 5(b). Two main peaks are observed, corresponding to the two different domains (either + c or $-c$) of the GaN wire. It is important to note that the histogram of the corrected phase shows sharper peaks. To calculate the phase shift between the two domains, the histograms of the corrected phase distribution have been fitted with two independent Gaussian curves:

$$f = \frac{A_1}{\sqrt{2\pi}\sigma_1} e^{-\frac{1}{2}\left(\frac{x-\mu_1}{\sigma_1}\right)^2} + \frac{A_2}{\sqrt{2\pi}\sigma_2} e^{-\frac{1}{2}\left(\frac{x-\mu_2}{\sigma_2}\right)^2}, \quad (2)$$

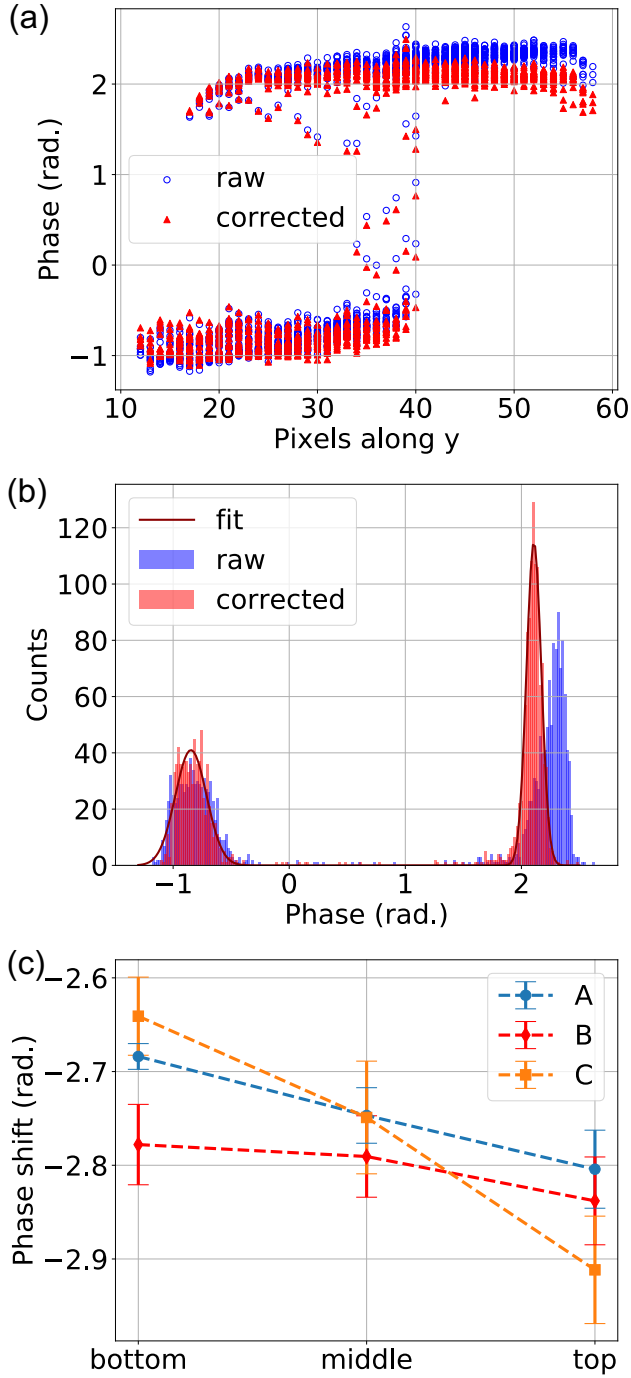


FIG. 5. (a) Raw and corrected values of the phase distribution along the y -axis of the reconstructed top cross-section of wire B . (b) Histograms of the phase of the raw and corrected (after optical path and phase ramp corrections) of the reconstructed top cross-section of wire B . Gaussian fit of the corrected phase histogram. (c) Evolution of the phase shift between inversion domains at the bottom, middle and top of the different wires.

where $A_{1,2}$, $\mu_{1,2}$ and $\sigma_{1,2}$ are the amplitude, central position of the peak and the standard deviation, respectively. The phase shift ($\mu_2 - \mu_1$) between the inversion domains at different po-

sitions along the wires is estimated from about 1200 different reconstructions (*i.e.*, 1200 different initial random phases), all of them showing a low value of their log-likelihood (LLK) metric.¹⁸ This allows to determine the average phase shift and its standard deviation (see Fig. 5(c)). The retrieved phase shift inversion domains is slightly different depending on the z -position along the wires. As an example, as reported in Fig. 5(c), the phase shift equals to -2.78 ± 0.04 rad., -2.79 ± 0.04 rad. and -2.84 ± 0.05 rad at the bottom, center and top parts of the wire B . A slight absolute increase of the phase-shift is thus observed from the bottom to the top for all the wires.

The reconstructions (Figs. 2, 3 and 4) clearly provide evidence of two types of domains of different phases. The phase values are rather constant inside the domains. The homogeneity of the phase inside the domains denotes the absence of significant strain variation. The phase difference between the domains partially originates in the phase difference of the structure factor between Ga and N-terminated GaN domains. Supposing that the Ga atoms are positioned in $(0,0,0)$ and $(\frac{1}{3}, \frac{2}{3}, \frac{1}{2})$ and N atoms in $(0,0,u_c)$ and $(\frac{1}{3}, \frac{2}{3}, \frac{1}{2} + u_c)$ in the unit cell for a Ga (+ c)-terminated domain and *vice versa* for a N (- c)-terminated domain, the structure factors of the + c and - c domains follow, for a given \mathbf{hkl} reflection:

$$\begin{aligned} \tilde{F}_{+c}(hkl) = & \tilde{f}_N(hkl) \cdot \{ \exp[Klu_c] + \exp[K(\frac{h}{3} + \frac{2k}{3} + \frac{l+2u_c}{2})] \} \\ & + \tilde{f}_{Ga}(hkl) \cdot \{ 1 + \exp[K(\frac{h}{3} + \frac{2k}{3} + \frac{l}{2})] \}, \end{aligned} \quad (3)$$

$$\begin{aligned} \tilde{F}_{-c}(hkl) = & \tilde{f}_{Ga}(hkl) \cdot \{ \exp[Klu_c] + \exp[K(\frac{h}{3} + \frac{2k}{3} + \frac{l+2u_c}{2})] \} \\ & + \tilde{f}_N(hkl) \cdot \{ 1 + \exp[K(\frac{h}{3} + \frac{2k}{3} + \frac{l}{2})] \}, \end{aligned} \quad (4)$$

where $K = -2i\pi$ and where $\tilde{f}_N(hkl)$ and $\tilde{f}_{Ga}(hkl)$ are the (complex) atomic scattering factors for N and Ga atoms, respectively. $u_c (= 0.377^{20})$ is the distance between two basal planes with atoms of different types in the wurtzite GaN unit cell. The diffracted amplitude of the wire with two domains (+ c and - c) can be written as:

$$\begin{aligned} \tilde{A}(hkl) \propto & \Omega_{+c} \cdot \tilde{F}_{+c}(hkl) \cdot FT[\exp(-i\vec{Q}_0 \cdot \vec{u}_{+c})] \\ & + \Omega_{-c} \cdot \tilde{F}_{-c}(hkl) \cdot FT[\exp(-i\vec{Q}_0 \cdot \vec{u}_{-c})] \\ \propto & FT[\Omega_{+c} \cdot \tilde{F}_{+c}(hkl) \cdot \exp(-i\vec{Q}_0 \cdot \vec{u}_{+c}) \\ & + \Omega_{-c} \cdot \tilde{F}_{-c}(hkl) \cdot \exp(-i\vec{Q}_0 \cdot \vec{u}_{-c})], \end{aligned} \quad (5)$$

where $\Omega_{+c}(\Omega_{-c}) = 1$ inside the + c (- c) domain and 0 outside, \vec{Q}_0 is the reference scattering vector in reciprocal space (corresponding to the measured \mathbf{hkl} reflection) and \vec{u}_{+c} , \vec{u}_{-c} are the atomic displacements of each domain. FT stands for Fourier transform. The retrieved complex-valued object then verifies:

$$\begin{aligned} \tilde{\Omega}(\vec{r}) = & \Omega_{+c} \cdot \tilde{F}_{+c}(hkl) \cdot \exp(-i\vec{Q}_0 \cdot \vec{u}_{+c}) \\ & + \Omega_{-c} \cdot \tilde{F}_{-c}(hkl) \cdot \exp(-i\vec{Q}_0 \cdot \vec{u}_{-c}). \end{aligned} \quad (6)$$

The difference of phase between the two domains, $\Delta\Phi$, originates from the difference of phase of the structure factor

between Ga (+c) and N (-c) terminated domains and from homogeneous displacement of the domains between each other:

$$\Delta\Phi_{-c \rightarrow +c} = \Phi_{\vec{F}_{-c}} - \Phi_{\vec{F}_{+c}} + \vec{Q}_0 \cdot (\vec{u}_{+c} - \vec{u}_{-c}). \quad (7)$$

Supposing that there is no homogeneous displacement between the +c and -c oriented domains, $\Delta\Phi_{-c \rightarrow +c} = 3.08$ rad. (or -3.2 rad.) for the **004** GaN reflection, the analytical atomic scattering factors of Ga and N being taken from the work of Waasmaier and Kirfel.²¹ The phase-shift observed for wire *B* varies from -2.78 ± 0.04 rad. (bottom) to -2.84 ± 0.05 rad (top). One has to introduce a rigid displacement of the atomic lattice between the two domains ($\vec{u}_{+c} - \vec{u}_{-c}$) in the *z* direction to match the experimental values. It varies from $(c/2+8.8) \pm 0.5$ pm (bottom) to $(c/2+7.5) \pm 0.5$ pm (top) for wire *B*. Wire *C* shows the largest variation: from $(c/2+6) \pm 1$ pm (bottom) to $(c/2+11.5) \pm 1.0$ pm (top). All these values are in good agreement with the additional shift of $c/2+8$ pm observed in Ref.⁹ From the obtained values, we can assert that for both wires, the domains in pink in Figs. 2 and 3 are -c (N-terminated) and the ones in green are +c (Ga-terminated).

The double polarity observed inside the GaN wires may originate at the interface between GaN and the sapphire substrate. The nucleation of the two polarities is expected to be initiated during the first stages of growth, during the steps of surface preparation and/or nucleation. When a polar layer is deposited on a non-polar substrate such as sapphire, it is the structure of the interface as well as the surface energies that will determine the polarity of the layer. In previous studies, surface nitriding conditions of the sapphire substrate and the growth conditions of the GaN buffer layer were identified as the parameters that can determine (and reverse) the polarity of the final layer.²² As well, as demonstrated by Romano *et al.*,²³ the formation of double polarity during the nucleation step of the GaN layer may result from the presence of inhomogeneities (atomic steps) at the GaN/sapphire surface.

The configuration of these two polar domains evolves along the GaN wires. This indicates that the IDBs change their direction of propagation, resulting in a variation in dimensions of the Ga- and N-terminated domains. As observed in Figs. 2 and 3, the size of the two domains varies along the growth axis of the wire. The expansion of the +c or Ga polar domain for both wires is in agreement with the usual tendency of this type of wire growth. It can be explained by the different speed of vertical and lateral growths of Ga polar domains compared to N polar domains.^{23,24}

It is worth noting that the IDBs at the top of the wire are all parallel to {1-100} or *m*-planes (see Fig. 3(b)). This is not the case at the bottom of the nanowire (see Fig. 3(f)). It is known that at the nanowire/substrate interface, dislocations occur due to the different lattice mismatch between the wire and substrate. The dislocation network may lead to a more complex IDB configuration. The IDBs adopt different configurations before stabilising into *m*-planes. The IDBs, separating the domains, correspond to {1-100} or *m*-planes as already observed in literature.²⁴⁻²⁶

Note that there is a discrepancy between the experimental and theoretical values of the phase shift expected between inversion domains. Experimentally, we observe an additional

shift of 8 ± 1 pm for the displacement along the *c*-axis. Simulations performed by Northrup *et al.*²⁷ and Labat *et al.*⁹ did not reproduce this additional shift. One possible explanation given by Labat *et al.*⁹ was the segregation of silicon atoms in the IDBs, as it is known that the presence of the silicon at an IDB modifies the bond length at the interface.²⁸ We have measured wires, for which the silane concentration has been varied (wires *B* and *C*) or not (wire *A*) during the growth. This has not impact on the displacement along the *c*-axis, implying that silicon has no noticeable effect on the displacement field generated by IDBs. Recently, Lançon *et al.*²⁹ have recovered the experimental small additional shifts of the polarity domains, in particular 8 pm shift along the hexagonal direction, by *ab initio* DFT calculations taking into account boundary conditions and electrostatic fields.

As a possible scenario, during the first seconds of nucleation, grains of different polarities are nucleated on the surface of the sapphire substrate. Over there the coalescence of grains leads to the appearance of a grain boundary and therefore the nucleation of an IDB between two domains of different polarities. The orientation of the IDB corresponds to the orientation of the coalescence boundary, which implies that it will not necessarily be in the (10 $\bar{1}$ 0) plane. The IDB may adopt different orientations. However, our observations show that the IDBs stabilise in the {10 $\bar{1}$ 0} planes. It is very likely that the fast vertical growth promotes the expansion of IDBs in the {10 $\bar{1}$ 0} planes. To explain the observed change of domain size, zigzag IDBs may form during growth.³⁰ Initially, the two polar domains are separated by IDBs. As Ga polar domains have a larger lateral growth, they will grow on the N polar domains. This leads to a change of configuration of the IDBs and probably the appearance of a zig-zag segment of IDB in the (0001) plane. This structural configuration is observed for all the measured wires.

In conclusion, we have studied the inversion domain boundary distribution in cross-sections of nanowires along their growth axis. This nm-resolved structural analysis provide understanding on their evolution along the nanowire. The IDBs were found to move along the growth axis, promoting Ga-terminated domains and stabilising into {1-100} or *m*-planes over N-terminated domains. The distance between domains was found to vary from $c/2+6$ to $c/2+11.5$ pm from top to bottom at maximum. The resolution on the displacement along the *c*-axis is a great advantage of Bragg coherent diffraction imaging compare with traditional microscopes. The technique offers a very precise inner view of the microstructure of small crystals in the presence of interacting defects. It can be also applied in a straightforward manner to materials under complex environment or *operando* as found in microelectronics and optoelectronics devices.

ACKNOWLEDGMENTS

The authors are grateful to ESRF Synchrotron for allocating beamtime. The measurement was performed at the ID01-ESRF beamline. We thank ID01 beamline staff for excellent support during the experiment and V. Favre-Nicolin for fruit-

ful discussions. This work has been funded by the French National Research Agency through the project ANR-11-BS10-01401 MecaniX. This project has also received funding from the European Research Council (ERC) under the European Union's Horizon 2020 research and innovation programme (grant agreement No. 818823).

- ¹S. Nakamura, T. Mukai, and M. Senoh, "Candela-class high-brightness InGaN/AlGaN double-heterostructure blue-light-emitting diodes," *Applied Physics Letters* **64**, 1687–1689 (1994).
- ²H. S. Jung, Y. J. Hong, Y. Li, J. Cho, Y.-J. Kim, and G.-C. Yi, "Photocatalysis Using GaN Nanowires," *ACS Nano* **2**, 637–642 (2008).
- ³S. Lester, F. Ponce, M. Craford, and D. Steigerwald, "High dislocation densities in high efficiency GaN-based light-emitting diodes," *Applied Physics Letters* **66**, 1249–1251 (1995).
- ⁴J. Basu, D. Ramachandran, S. Kumar, and C. Carter, "Inversion Domain Boundaries in Wurtzite GaN," *Microscopy and Microanalysis* **12**, 1084–1085 (2006).
- ⁵F. Glas, "Critical dimensions for the plastic relaxation of strained axial heterostructures in free-standing nanowires," *Phys. Rev. B* **74**, 121302 (2006).
- ⁶H. D. Espinosa, R. A. Bernal, and M. Minary-Jolandan, "A review of mechanical and electromechanical properties of piezoelectric nanowires," *Advanced Materials* **24**, 4656–4675 (2012), <https://onlinelibrary.wiley.com/doi/pdf/10.1002/adma.201104810>.
- ⁷J. Chesin and S. Gradecak, "Comparing directed efficiency of III-nitride nanowire light-emitting diodes," *Journal of Nanophotonics* **8**, 1–14 (2014).
- ⁸I. Robinson and R. Harder, "Coherent X-ray diffraction imaging of strain at the nanoscale," *Nature Materials* **8**, 291–298 (2009).
- ⁹S. Labat, M.-I. Richard, M. Dupraz, M. Gailhanou, G. Beutier, M. Verdier, F. Mastropietro, T. W. Cornelius, T. U. Schüllli, J. Eymery, and O. Thomas, "Inversion Domain Boundaries in GaN Wires Revealed by Coherent Bragg Imaging," *ACS Nano* **9**, 9210–9216 (2015).
- ¹⁰A. Ulvestad, A. Singer, J. N. Clark, H. M. Cho, J. W. Kim, R. Harder, J. Maser, Y. S. Meng, and O. G. Shpyrko, "Topological defect dynamics in operando battery nanoparticles," *Science* **348**, 1344–1347 (2015).
- ¹¹F. Hofmann, E. Tarleton, R. J. Harder, N. W. Phillips, P.-W. Ma, J. N. Clark, I. K. Robinson, B. Abbey, W. Liu, and C. E. Beck, "3d lattice distortions and defect structures in ion-implanted nano-crystals," *Scientific Reports* **7**, 45993 (2017).
- ¹²O. Mandula, M. Elzo Aizarna, J. Eymery, M. Burghammer, and V. Favre-Nicolin, "PyNX.Ptycho: a computing library for X-ray coherent diffraction imaging of nanostructures," *Journal of Applied Crystallography* **49**, 1842–1848 (2016).
- ¹³D. R. Luke, "Relaxed averaged alternating reflections for diffraction imaging," *Inverse Problems* **21**, 37–50 (2004).
- ¹⁴R. Gerchberg and O. Saxton, "A practical algorithm for the determination of the phase from image and diffraction plane pictures," *Optik* **35**, 237–246 (1972).
- ¹⁵J. Fienup, "Phase Retrieval Algorithms - a Comparison," *Applied Optics* **21**, 2758–2769 (1982), wOS:A1982PB81000030.
- ¹⁶S. Marchesini, H. He, H. N. Chapman, S. P. Hau-Riege, A. Noy, M. R. Howells, U. Weierstall, and J. C. H. Spence, "X-ray image reconstruction from a diffraction pattern alone," *Physical Review B* **68**, 140101 (2003).
- ¹⁷J. R. Fienup and C. C. Wackerman, "Phase-retrieval stagnation problems and solutions," *JOSA A* **3**, 1897–1907 (1986).
- ¹⁸P. Thibault and M. Guizar-Sicairos, "Maximum-likelihood refinement for coherent diffractive imaging," *New Journal of Physics* **14**, 063004 (2012).
- ¹⁹R. Harder, M. A. Pfeifer, G. J. Williams, I. A. Vartaniants, and I. K. Robinson, "Orientation variation of surface strain," *Physical Review B* **76**, 115425 (2007).
- ²⁰H. Schulz and K. H. Thiemann, "Crystal structure refinement of AlN and GaN," *Solid State Communications* **23**, 815–819 (1977).
- ²¹D. Waasmaier and A. Kirfel, "New analytical scattering-factor functions for free atoms and ions," *Acta Crystallographica Section A Foundations of Crystallography* **51**, 416–431 (1995).
- ²²N. Stolyarchuk, T. Markurt, A. Courville, K. March, O. Tottreau, P. Vennéguès, and M. Albrecht, "Impact of sapphire nitridation on formation of Al-polar inversion domains in N-polar AlN epitaxial layers," *Journal of Applied Physics* **122**, 155303 (2017).
- ²³L. T. Romano, J. E. Northrup, and M. A. O'Keefe, "Inversion domains in GaN grown on sapphire," *Applied Physics Letters* **69**, 2394–2396 (1996).
- ²⁴X. H. Wu, P. Fini, S. Keller, E. J. Tarsa, B. Heying, U. K. Mishra, S. P. DenBaars, and J. S. Speck, "Morphological and Structural Transitions in GaN Films Grown on Sapphire by Metal-Organic Chemical Vapor Deposition," *Japanese Journal of Applied Physics* **35**, L1648 (1996).
- ²⁵A. R. Head, S. Chaudhary, G. Olivieri, F. Bournel, J. N. Andersen, F. Rochet, J.-J. Gallet, and J. Schnadt, "Near Ambient Pressure X-ray Photoelectron Spectroscopy Study of the Atomic Layer Deposition of TiO₂ on RuO₂(110)," *The Journal of Physical Chemistry C* **120**, 243–251 (2016).
- ²⁶S. Keller, C. S. Suh, N. A. Fichtenbaum, M. Furukawa, R. Chu, Z. Chen, K. Vijayaraghavan, S. Rajan, S. P. DenBaars, J. S. Speck, and U. K. Mishra, "Influence of the substrate misorientation on the properties of N-polar InGa_N/Ga_N and AlGa_N/Ga_N heterostructures," *Journal of Applied Physics* **104**, 093510 (2008).
- ²⁷J. Northrup, J. Neugebauer, and L. Romano, "Inversion Domain and Stacking Mismatch Boundaries in GaN," *Physical Review Letters* **77**, 103–106 (1996).
- ²⁸P. Gibart, "Metal organic vapour phase epitaxy of GaN and lateral overgrowth," *Reports on Progress in Physics* **67**, 667–715 (2004).
- ²⁹F. Lançon, L. Genovese, and J. Eymery, "Towards simulation at picometer-scale resolution: Revisiting inversion domain boundaries in GaN," *Physical Review B* **98** (2018), 10.1103/PhysRevB.98.165306.
- ³⁰A. P. Goldstein, S. C. Andrews, R. F. Berger, V. R. Radmilovic, J. B. Neaton, and P. Yang, "Zigzag Inversion Domain Boundaries in Indium Zinc Oxide-Based Nanowires: Structure and Formation," *ACS Nano* **7**, 10747–10751 (2013).